Polymer Testing 137 (2024) 108524

Contents lists available at ScienceDirect

Polymer Testing

journal homepage: www.elsevier.com/locate/polytest

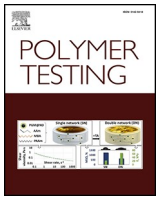

Combining fast scanning chip calorimetry and nanoindentation: Young's modulus and hardness of poly (L-lactic acid) containing α′- and α-crystals

Katalee Jariyavidyanont [a,*], Christina Wüstefeld [b], Thomas Chudoba [c], René Androsch [a,**]

[a] Interdisciplinary Center for Transfer-oriented Research in Natural Sciences (IWE TFN), Martin Luther University Halle-Wittenberg, 06099, Halle, Saale, Germany
[b] Institute of Materials Science, TU Bergakademie Freiberg, Gustav-Zeuner-Str. 5, 09599, Freiberg, Germany
[c] ASMEC GmbH, Maria-Reiche-Str. 1, 01109, Dresden, Germany

ARTICLE INFO

Keywords:
Nanoindentation
Fast scanning chip calorimetry
Young's modulus
Indentation hardness
Crystal polymorphism
Poly (L-lactic acid)

ABSTRACT

Fast scanning chip calorimetry (FSC) allows subjecting polymer melts to well-defined vitrification, crystal nucleation, and crystal growth pathways and, therefore, precise control of morphologies, from fully amorphous glassy states to semicrystalline structures containing perfect crystals. Due to the required use of nanogram-sized samples, needed to achieve high cooling rates, their mechanical properties, in order to establish structure-property relations, are difficult to assess. In this work, indentation modulus and indentation hardness of FSC samples are successfully determined on example of semicrystalline poly (L-lactic acid) (PLLA) containing spherulitically grown disorder α′- or rather perfect α-crystals, with the correctness of the applied preparation and analyses routes confirmed by nanoindentation measurements on milligram-sized samples prepared through hotstage microscopy, and by applying both static single-step and quasi-continuous stiffness measurements. Modulus and hardness data are consistent with prior analyses of bulk samples, confirming that semicrystalline PLLA containing α-crystals exhibits around 10–20 % higher values of these properties compared to PLLA containing α′-crystals, related to the different molecular-chain packing in the crystal lattice. This work demonstrates that combination of FSC and nanoindentation techniques is an effective tool for determining mechanical properties of samples solidified at specific thermal pathways which otherwise cannot be realized.

1. Introduction

Knowledge of the properties of polymers is crucial for customizing their macroscopic behavior to meet specific application requirements. Among those, the mechanical properties are of superior importance for many engineering but also daily-life uses, which, for a given polymer, depend on the supermolecular structure/morphology. This includes the fraction, structure, size, and spatial arrangement of crystals in case of semicrystalline polymers, or the structure of the glass in case of amorphous polymers [1–6]. All of these structural features are controlled and adjustable by the conditions of solidification/crystallization of the melt, for example the cooling rate [7–10].

Mechanical properties of polymeric materials often are obtained from macroscopic bulk samples, prepared, for example, by injection molding. However, due to the combined action of shear and cooling during processing, being different in the various locations of a molding, often gradient-structures develop, well known as skin-core morphology [11–13]. These can include gradients in the crystallinity, the orientation and morphology of crystals, or even their polymorphic state, affecting mechanical properties, which typically represent then an average of different contributions when measured e.g. by classical tensile stress-strain testing [14–16], not allowing to obtain well defined structure-property relations. Attempts to assess the local properties of such gradient-samples include preparation and analysis of sliced thin sections [17–19], or μm-scale position-resolved indentation tests [20, 21]. Alternatively, to avoid the need of analysis of inhomogeneous samples, structure-gradient-free films of rather low thickness with a specific solidification history, including conditions as in melt processing, were investigated [22–26]. However, both analysis routes for obtaining structure-specific mechanical properties, that is, preparation of specimens from conventionally melt-processed macroscopic samples, or of rather thin films (of the order of magnitude of few 10–100 μm, to assure absence of structural gradients), lack realization of well-defined solidification conditions. Application of instrumentation, which subjects

* Corresponding author.
** Corresponding author.
E-mail address: katalee.jariyavidyanont@iw.uni-halle.de (K. Jariyavidyanont).

https://doi.org/10.1016/j.polymertesting.2024.108524
Received 2 May 2024; Received in revised form 3 July 2024; Accepted 18 July 2024
Available online 20 July 2024

small samples to precise cooling/solidification profiles, as is available with fast scanning chip calorimetry (FSC) [27], may overcome this shortcoming.

FSC, due to the low mass of samples of the order of magnitude of few to 100 ng, and due to the smallness of the calorimeter, permits heating and cooling at rates up to —depending on the specific instrumentation used— 10^8 K/s [27–29], covering the conditions typically evident in polymer processing [30–34]. With this opportunity, starting from the relaxed melt, any structural state —from glasses of different metastability to semicrystalline states containing crystals formed at any supercooling— can be adjusted. While calorimeters mainly serve for precise measurement of heat-flow rates from/to samples in response to an imposed thermal profile [35], there is increasing interest to analyze FSC samples, both in- and ex-situ, by complementary tools for gaining additional information about the structure. These include polarized-light optical microscopy [36,37], atomic force microscopy [38,39], electron microscopy [40,41], wide- and small-angle X-ray scattering [42–44], or infrared spectroscopy [45,46]. With that, detailed structure information of specifically solidified materials is available, however, to the best of our knowledge, mechanical analysis of FSC samples is not yet reported, being therefore subject of the present work. The small size of the FSC samples —being at best few μm thick and few ten μm wide— exclude classical macroscopic testing methods for characterization of their mechanical behavior rather than requires application of techniques operating at the nanometer length scale. Among those, nanoindentation appears being a promising tool as it allows assessing mechanical properties at specific positions, at least, at the μm-scale, and, importantly, requires only small area/volume for measurement [47–49].

In this work, we use poly (L-lactic acid) (PLLA) for testing the application of nanoindentation measurements for gaining information about the mechanical behavior of FSC samples. PLLA is a biobased and biodegradable polymer produced by polycondensation of plant-based lactic-acid monomers derived from corn, potatoes, and sugarcane resources [50–52], and its glass transition temperature (T_g) and equilibrium melting temperature ($T_{m,0}$) are about 60 and 200 °C, respectively [53–55]. PLLA is a rather slow crystallizing polymer [56–58] and exhibits crystal polymorphism [59,60]. Melt-crystallization at temperatures below about 100 °C or higher than 120 °C leads to formation of α′- or α-crystals, respectively, while both crystal forms grow between 100 and 120 °C [61–63]. The α-phase exhibits an orthorhombic crystal structure [64,65], while the unit cell of α′-crystals is orthorhombic [65,66] or pseudo-hexagonal [67,68]. In the α′-crystal polymorph, distances between neighbored molecules are slightly larger compared to the α-phase, and the chains contain conformational defects/distortions [67–69], causing a decrease of the temperature and enthalpy of melting, and affecting all material properties [70–73]. The mechanical properties depend on the crystal fraction in the overall semicrystalline structure, with PLLA containing α-crystals showing a higher Young's modulus and lower elongation at break than PLLA containing disorder α′-crystals [73–75]. Moreover, analysis of samples of different crystallinity, in combination with modelling or extrapolation procedures, allowed assessing Young's modulus of the individual crystal phases [75,76]. Though different values were obtained in the various studies, data consistently proof a higher value of Young's modulus of α-crystals compared to α′-crystals, being in qualitative agreement with theoretical calculations [77,78]. Our own work employed isotropic and gradient-free films for analysis of Young's modulus, with the crystallinity adjusted in a wide range from zero to about 75 %, and assuring identical superstructures of samples containing different crystal polymorphs, achieved using special nucleation, crystallization and crystal-reorganization pathways [76]. As such, values of Young's modulus of about 3.7 and 4.6 GPa for isotropic aggregations of α′- and α-crystals —both being of lamellar shape [79]— respectively, were suggested. These values are only slightly higher than Young's modulus of the unaged amorphous PLLA glass of around 3.0 GPa, which, however, slightly increases over time during physical aging [6,76,80–82].

Based on this information, PLLA containing different crystal polymorphs is selected serving as test object for analysis of indentation modulus and hardness by nanoindentation on nanogram-sized samples after preparation/crystallization along specific thermal pathways in an FSC. As such, also a comparison of intraspherulitically observed local mechanical properties (by nanoindentation) and global mechanical properties obtained (by dynamic-mechanical analysis) as average value of polyspherulitic macroscopic films, available in the literature [76], is possible. In addition, we applied nanoindentation on microgram-sized samples prepared by hotstage microscopy, to assure reliability of measurements performed on FSC samples.

2. Experimental

2.1. Material

An extrusion grade PLLA from Corbion (The Netherlands), delivered in form of pellets, was used in this work. It is a homopolymer containing less than 1 % D-isomers, and has a melt-flow rate of 8 g/(10 min) (210 °C/2.16 kg) [83]. The mass-average molar mass of the used polymer is 120 kg/mol [84].

2.2. Preparation of samples by hotstage microscopy

Thin sections with a thickness of about 50 μm and a lateral width of 2–3 mm were prepared from the cross section of as-received pellets using a CUT-5062 rotary microtome (Slee, Mainz, Germany), placed onto a circular glass, and then put onto a THMS600 hotstage (Linkam, Tadworth, United Kingdom). The hotstage was attached on the sample stage of a DMRX polarized-light optical microscope (POM) (Leica, Wetzlar, Germany). After preparing the samples at defined protocols (described in detail below), we captured an overview of their structures at room temperature using a Nikon DS-Fi3 camera attached to an Eclipse LV100 N POL optical microscope (Nikon, Düsseldorf, Germany) in transmission mode, using crossed polarizers. The Results and Discussion section, below, provides further details regarding the thermal profiles applied to obtain different polymorphic structures.

For nanoindentation experiments, the circular glass with the sample on top was fixed onto a cylindrical steel-stub, serving as sample stage/holder, using CrystalBond™ 555 (polyolefin wax). For this, first the steel-stub was heated on a hotplate to 57 °C, being slightly above the melting temperature of the adhesive, and afterward, it was distributed/melted by rubbing it on the hot surface of the steel-stub. Then, immediately after removal the steel sample holder from the hotplate, the circular glass with the samples was gently pressed onto the still molten CrystalBond™ 555 film, followed by natural cooling to room temperature by the surrounding atmosphere, allowing solidification of CrystalBond™ to function as an adhesive between the glass and the sample holder. It is important noting that the melting temperature of the selected CrystalBond™ adhesive is slightly lower than the glass transition temperature of PLLA. Thus, reheating the sample while gluing the glass substrate to the metal stub does not alter the supermolecular structure of the polymer.

2.3. Preparation of FSC samples

For crystallization experiments, we used a Flash DSC 2+ (Mettler-Toledo, Greifensee, Switzerland) in combination with (conditioned and temperature-corrected [85]) UFS 1 chip sensors, with the instrument connected to an intracooler TC100 (Huber, Offenburg, Germany), assuring a constant sample-support temperature of −90 °C for fast and controlled cooling of samples and realization of melt-crystallization along well-defined thermal pathways. The sensor compartment was purged with nitrogen gas at a flow rate of about 40 mL/min, to avoid

thermal-oxidative degradation of the polymer and moisture condensation. Thin sections with a thickness of about 20 μm were cut from the as-received PLLA pellets with a microtome (Slee, Mainz, Germany) and then their lateral size was reduced to few hundred micrometers, to not exceed the heatable area of the sensor. A thin layer of silicone oil, distributed on the sensor membrane prior loading a sample served to improve the thermal contact. For ex-situ observation of the microstructure of the FSC samples after crystallization, we employed an OPN-184 microscope (Kern, Bahlingen, Germany) in reflection mode, using crossed polarizers. A DFK 33UX252 digital camera (Imaging-Source, Bremen, Germany), attached to the microscope, allowed taking micrographs of the samples.

Analysis of mechanical properties of FSC samples by nanoindentation requires a separate preparation step since the sample typically is not removable from the active/heatable area of the UFS 1 sensor. For illustration, Fig. 1 shows a schematic view of the sensor cross-section (top), a photograph of the sensor showing the sample and reference furnaces embedded in a ceramic support (bottom left), and a photograph of a typical polymer sample placed on the heatable area of the sample furnace (bottom right); further sensor images are available in the literature [86,87]. The sketch at the top shows that the sample is located on a freestanding silicon nitride/oxide membrane with a thickness and area of 2.1 μm and 1.6 × 1.6 mm^2, respectively, containing resistance heaters and thermopiles for temperature measurements. The circular active area is located in the center of the membrane, with a diameter of 500 μm, containing an aluminum coating, for achieving a rather homogeneous temperature field [86–88]. The bottom-left photograph illustrates that the UFS 1 sensor contains two thermally decoupled furnaces, serving as sample and reference calorimeters, all embedded in a silicone frame and ceramic support for easy handling. Further details about the UFS 1 are available elsewhere [86,87,89].

Direct measurement of mechanical properties of FSC samples by nanoindentation is complicated due to the fragility and mechanical instability of the membrane but also the height difference of around 1 mm between the ceramic support and the sample surface, not allowing proper positioning of the nanoindenter. Loading samples on the backside of the sensor membrane may avoid the geometrical constraint of reaching the sample surface with the indenter, however, the mechanical instability of the membrane still requires placing it onto a solid and

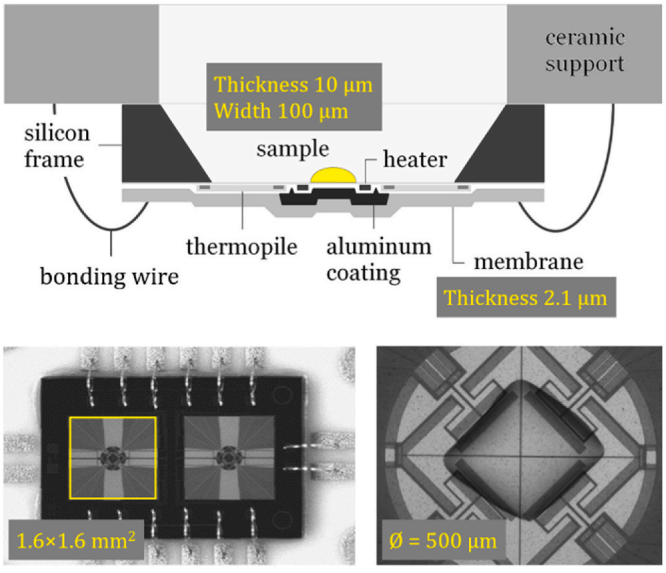

Fig. 1. UFS 1 chip sensor used for preparation of PLLA for subsequent analysis of indentation modulus and hardness. Schematic view of the sensor cross-section (top), bottom view of the sample and reference calorimeters (bottom left) and typical polymer sample in the center of the heatable area of the sensor (bottom right). Images adapted with permission from Refs. [87,90,91].

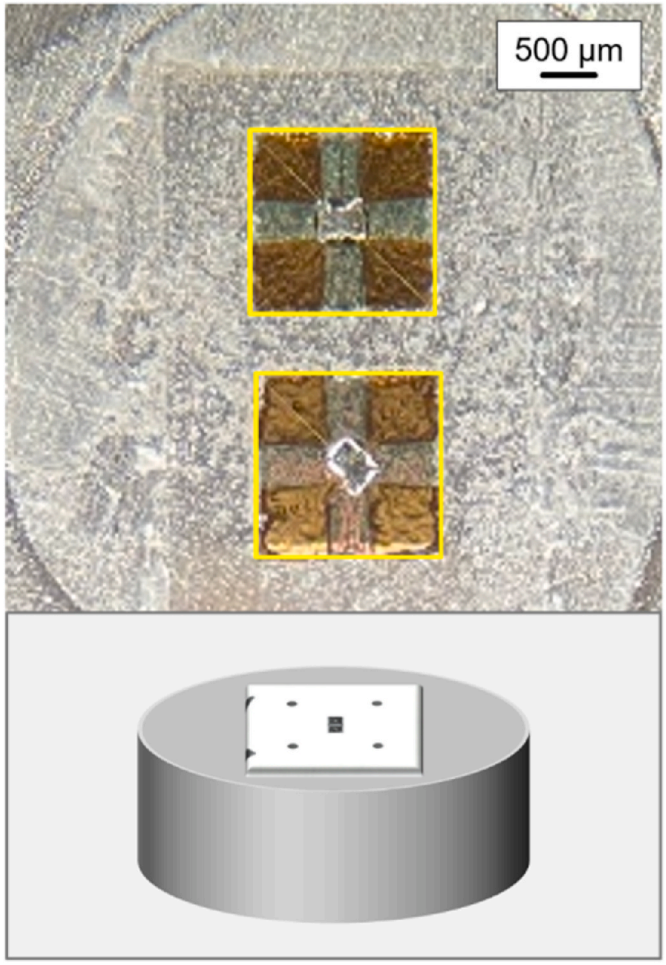

Fig. 2. Schematic of a UFS 1 chip sensor (including the sample under investigation) mounted at 57 °C on a steel-stub/sample holder using CrystalBond™ 555 as adhesive (bottom). UFS-1 chip sensor membranes (with sample) after removal of the ceramic frame at ambient temperature (top).

sufficiently stiff substrate. Therefore, we removed both the ceramic support and silicon frame and adhered the membrane, containing the sample, to the steel sample holder, as illustrated with Fig. 2. First, the bonding wires, connecting the membrane and electrical contacts at the ceramic frame (see Fig. 1, bottom left) were removed. Then, similar as in case of preparation of hotstage-crystallized samples for nanoindentation, CrystalBond™ 555 served as adhesive for mounting the chip sensor at its backside at 57 °C. After cooling to ambient temperature —causing solidification/crystallization of the adhesive— we pulled off the ceramic and silicon frames, leaving only the sensor membrane with the sample on the metal sample holder. Fig. 2 shows in the bottom part a sketch of the UFS-1 chip sensor (including the sample under investigation) as mounted at 57 °C, using CrystalBond™ 555 as adhesive, on the steel sample holder of the nanoindenter-device described below. The top part is a photograph of the UFS-1 chip sensor sample- and reference-side membranes (see yellow framed areas), containing the sample, after removal/pulling off the ceramic frame at ambient temperature.

2.4. Nanoindentation

We employed a ZwickRoell ZHN nanoindenter (Ulm, Germany) for analysis of the mechanical properties of PLLA samples. The measurements were performed at room temperature using a Berkovich indenter (tip radius <200 nm, Young's modulus 1140 GPa, Poisson ratio 0.07) and applying two different measurement protocols to ensure reliability

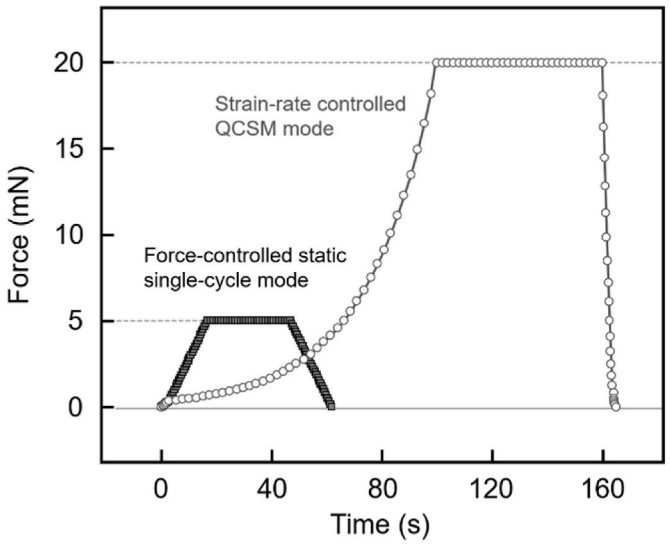

Fig. 3. Load-time profiles for nanoindentation experiments using force-controlled single cycle (black) and strain-rate controlled quasi-continuous stiffness measurement (gray) modes. Axis numbers only hold for single-step measurements.

of observed data and to obtain additional information about the depth-dependence of properties. Fig. 3 shows the load-time profiles of a force-controlled quasi-static single-cycle test (black curve) and a strain-rate controlled dynamic quasi-continuous stiffness measurement (QCSM) (gray). Regarding the single-cycle test [92], after an initial surface-approach segment, the load is linearly increased to a maximum value of 5 mN within 15 s, kept constant for 30 s to detect possible creep, followed by unloading at the same rate as loading was done. We performed experiments with and without a second holding-step of 20 s at 10 % of the maximum force, which, however, revealed only negligible effect on modulus data because it was not used for thermal drift correction and had no influence on the slope of the unloading curve. Averages of the analyzed mechanical properties of the various phases of PLLA were determined based on 20 to 80 individual measurements.

In QCSM tests, a dynamic force is superimposed to the static force by a sinusoidal oscillation. The method uses a stepwise loading with the oscillation turned off between the static load steps. Oscillation starts only when the predefined force step is reached. 40 load steps (points) up to a maximum force of 20 mN have been used employing an exponential loading function, resulting in a constant strain rate of about 0.02 1/s. 30 points have been measured during the creep step of 60 s while keeping the force constant at 20 mN. The oscillation frequency was 40 Hz, the dwell time per point was 1.4 s, and the displacement amplitude varied between 1.5 and 3 nm.

In QCSM mode, the force of every single point is exactly controlled and therefore all points in the loading segment experience the same force in repeated tests within a few-μN accuracy so that an averaging of several measurements is allowed. The given results represent average data from 6 to 10 single measurements. The error bars indicate the statistical uncertainty obtained from the standard deviations of depth, force, time and stiffness per point. In contrast to a single-cycle measurement, a QCSM measurement provides the indentation hardness and indentation modulus as a function of the penetration depth [92–95]. However, the indentation hardness is the hardness before creep (beside the points from the creep segment) while single-cycle measurements always yield the hardness after creep. For the calculation of the modulus, we assumed a Poisson's ratio of PLLA of 0.35.

The conventional evaluation of the load–displacement curves, using the slope of the unloading segment, was done according to the standard ISO 14577:2015 (Oliver and Pharr method with additional radial displacement and variable epsilon factor correction) [96–98]. The indentation modulus corresponds to Young's modulus when disturbing effects like pile-up or sink-in can be neglected.

All nanoindentation tests were performed on samples aged for several days, to assure a quasi-metastable structural state and allowing therefore comparison of mechanical properties.

3. Results and discussion

3.1. Nanoindentation of hotstage-prepared PLLA samples containing different crystal polymorphs

Fig. 4 shows temperature-time protocols for preparation of PLLA films/sections of 50 μm thickness placed on glass coverslips, serving as substrate. The two thermal profiles allow generation of multiphase structures containing different crystal polymorphs and amorphous glassy phases in different environments, all expected to exhibit different mechanical behaviors. First, the thin sections were heated to 220 °C, that is, to above $T_{m,0}$ [53,54], and equilibrated at this temperature for 3 min. This step is followed by isothermal crystallization of the melt at 140 °C for 90 min (see red segment), with the crystallization temperature approached by fast cooling the melt at 50 K/min, suppressing non-isothermal crystallization [99,100]. Crystallization at 140 °C for 90 min yields spherulitically grown lamellar α-crystals, however, with the pre-selected crystallization time of 90 min too short to achieve a space-filled spherulitic structure, leaving non-crystallized material outside the spherulites for further thermal treatments, as illustrated with pathways (a) or (b) in Fig. 4. Quenching the sample to room temperature (RT), as realized with path (a), that is to below T_g of about 60 °C [53–55], caused vitrification of non-crystallized material in both inside and outside the spherulites. In case of pathway (b), after crystallization at 140 °C and rapid cooling the sample to 90 °C at 50 K/min, the still available interspherulitic space was allowed to continue to crystallize for 120 min, however, leading now to space-filling formation of spherulitically grown disorder α′-crystals (see blue segment). The preparation of samples containing different structures, we consider advantageous for comparison of their mechanical properties, due to minimizing errors, e.g., when using different substrates or samples of different thickness.

Fig. 5 shows with the left and right POM-images examples of the micrometer-scale structure of PLLA crystallized along the thermal pathways (a) and (b) of Fig. 4, respectively. As such, the left image reveals the presence of rather large spherulites with a diameter of about

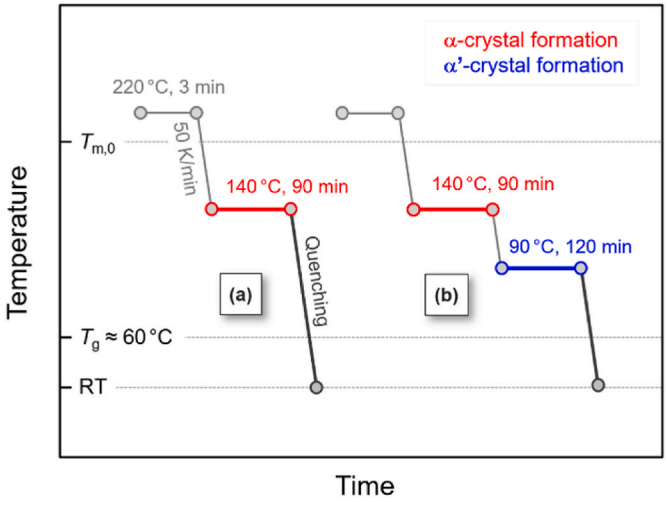

Fig. 4. Temperature-time protocols for preparation of PLLA containing α-crystals and intra- and interspherulitic amorphous structure [path (a)] and α-crystals, α′-crystals, and intraspherulitic amorphous structure [path (b)], both prepared by hotstage microscopy.

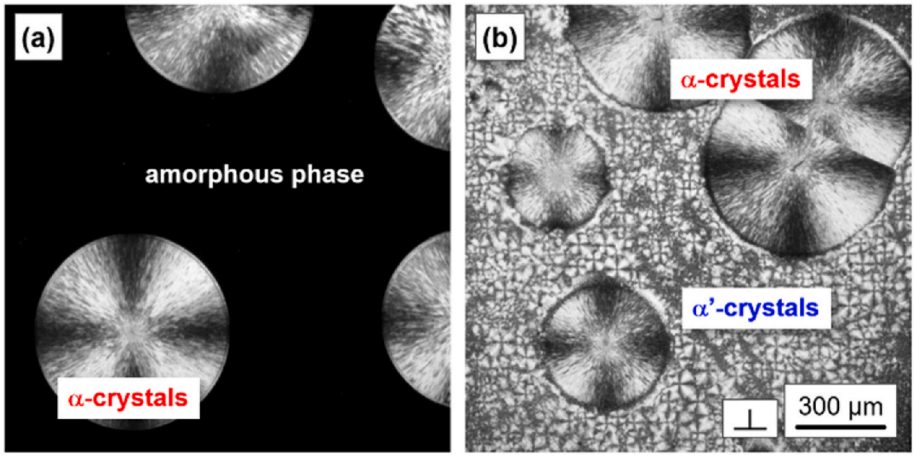

Fig. 5. POM images of PLLA samples prepared by hotstage microscopy, crystallized according to temperature-time protocols/pathways (a) (left image) and (b) (right image) (see also Fig. 4). The scale bar holds for both images, and the polarizer directions are oriented parallel to the image borders as indicated to the left of the scale bar.

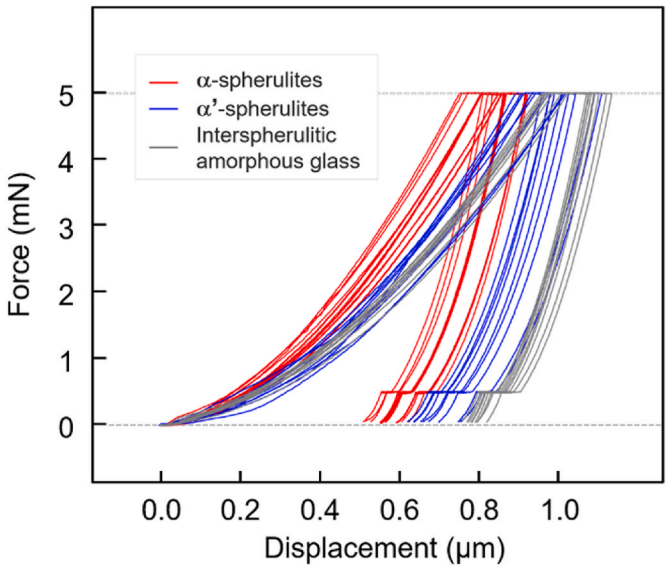

Fig. 6. Force-displacement curves obtained by the quasi-static single test method on PLLA sections with a thickness of 50 μm on a glass substrate, prepared along the crystallization pathways (a) and (b) in Fig. 4.

0.5 mm, containing α-crystals formed at 140 °C and intraspherulitic amorphous structure, both not resolvable by optical microscopy but higher magnification imaging techniques [79]. These spherulites are embedded in glassy amorphous (interspherulitic) PLLA, as was achieved by quenching the polymer to below T_g, appearing black when imaged with crossed polarizers.

In case of the sample prepared along pathway (b), similarly large spherulites containing α-crystals are present, which, however, are now neighbored by distinctly smaller spherulites with a size of the order of magnitude of only 10 μm, as formed by the additional crystallization step at 90 °C, containing disorder α′-crystals and amorphous structure. Note that the increase of the number of crystal nuclei on lowering the crystallization temperature causes the difference in the size and number of spherulites grown at 140 and 90 °C [101].

Samples as shown in Fig. 5 are then used for position-resolved nanoindentation measurements for analysis of the hardness and modulus (i) of glassy amorphous PLLA (black area in the left image of Fig. 5), (ii) of (large) spherulites containing α-crystals and intraspherulitic glassy amorphous structure, and (iii) of (small) spherulites containing disorder α′-crystals and intraspherulitic glassy amorphous structure. Again, as the structure of the amorphous glass depends on time, affecting mechanical properties, samples were stored at ambient temperature for several days, assuring a close-to metastable structural state [6]. In addition, with the thermal profiles of Fig. 4, we achieved that the (local) crystallinity in spherulites containing either α′- or α-crystals is similar —being around 60 %— since these spherulites were not subjected to extended secondary crystallization at the crystallization temperature.

Fig. 6 shows sets of force-displacement curves, obtained by the quasi-static single-cycle method, of PLLA samples crystallized along the crystallization pathways (a) and (b) (see Fig. 4). Red and blue curves are related to indentations within α- and α′-spherulites, respectively, while the gray curves were collected by indentation into the bulk amorphous interspherulitic glass (see also Fig. 5). Albeit curves, which are associated to a specific structure, exhibit statistics, obviously the various analyzed structures show a different mechanical behavior, as seen by the different displacement/indentation depth at the maximum applied load of 5 mN. Visual inspection of the curves suggests that the modulus and hardness of α-crystals containing spherulites is larger than in case of spherulites containing α′-crystals or in case of the bulk (interspherulitic) amorphous glass. In detail, the average hardness and indentation

Table 1
Indentation hardness and modulus of bulk (non-intraspherulitic) amorphous structure and semicrystalline PLLA spherulites containing different crystal polymorphs prepared by hotstage microscopy and analyzed *via* single-cycle and QCSM test methods. The data obtained from the QCSM method correspond to the last right points in Fig. 7.

Sample	Single-cycle method		QCSM method	
	Hardness (GPa)	Modulus (GPa)	Hardness (GPa)	Modulus (GPa)
Bulk amorphous phase	0.20 ± 0.01	4.7 ± 0.1	0.19 ± 0.01	5.0 ± 0.1
α′-form spherulites	0.25 ± 0.04	4.8 ± 0.3	0.22 ± 0.01	4.9 ± 0.2
α-form spherulites	0.30 ± 0.03	6.0 ± 0.4	0.26 ± 0.08	5.8 ± 0.1
α-form spherulites (by reorganization)	–	–	0.26 ± 0.01	5.6 ± 0.2

modulus of α-spherulites are 0.30 and 6.0 GPa, respectively, for α′-spherulites 0.25 and 4.8 GPa, and for the bulk amorphous glass 0.20 and 4.7 GPa. More information, including errors, is provided in Table 1, below, together with data obtained by QCSM.

The higher modulus/hardness for PLLA containing the more perfect α-crystals, compared to PLLA containing disorder α′-crystals, is expected from prior, macroscopic mechanical tests, and is related to their higher intrinsic stiffness [75–77]. Furthermore, from these prior experiments, it is also expected that the amorphous glass has a lower modulus than semicrystalline structure [76,77,102], which is also observed here. However, regarding the rather small difference of the modulus of the amorphous glass and spherulitic structure containing α′-crystals, it should be noted that all samples were analyzed after long-term storage at ambient temperature, slightly below the glass transition temperature. This causes physical aging including enthalpy-relaxation and densification of the amorphous glass, increasing both hardness and modulus by 10–20 % [5,6], justifying the experimental observations here.

The reproducibility of observations described above, we confirmed by performing analyses on up to four individual samples and indentations in different sample areas. The reliability of data obtained by single-cycle nanoindentation tests, we checked furthermore by QCSM experiments, with the particular intension to exclude errors due to the indentation-size effect [103–105]. The indentation-size effect describes the increase of the hardness and modulus with decreasing depth of indentation below few μm. Since the maximum load of 5 mN in the single-cycle test gave only a maximum displacement of the indenter of about 1 μm (see Fig. 6) no statement can be made about a variation of hardness with depth. This, however is possible by the QCSM measurements.

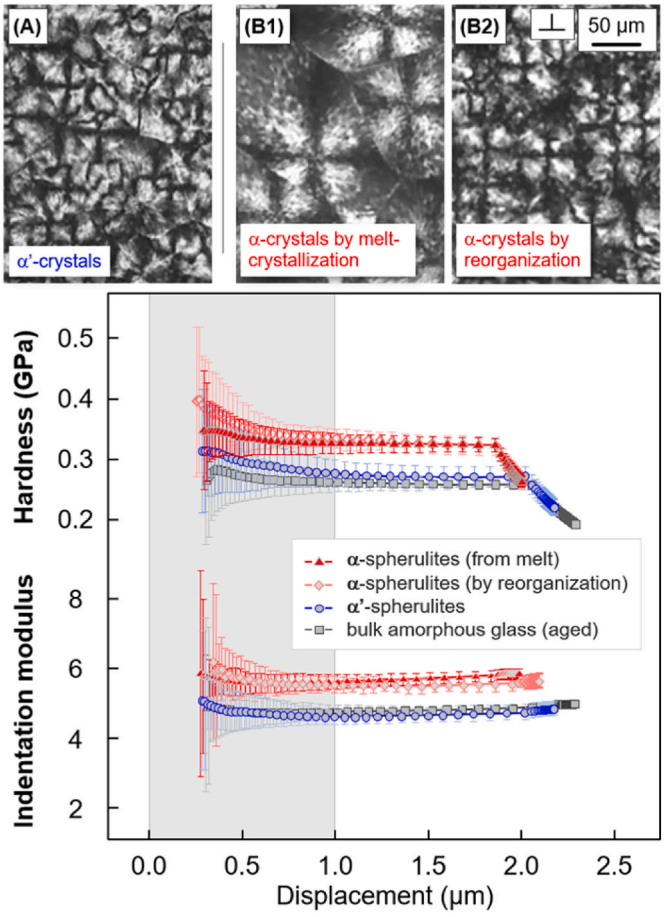

Fig. 7. POM images of the μm-scale structure of PLLA containing α′-crystals grown from the melt at 90 °C (A) (left), and of PLLA containing α-crystals formed by direct transformation of the melt at 130 °C (B1) (center), or by a solid-solid phase transformation of α′-crystals (B2) (right) (top). The scale bar holds for all images and the polarizer directions are oriented parallel to the image borders. Hardness and indentation modulus of different PLLA structures, as indicated in the legend, as a function of the indentation depth/displacement (bottom).

Fig. 7 shows in the top part different semicrystalline morphologies of PLLA, again prepared using the hotstage-sample-preparation route. The left image (A) reveals the structure of semicrystalline PLLA containing spherulitically grown α′-crystals obtained by isothermal melt-crystallization at 90 °C until space filling, while the center and right micrographs show the structure of PLLA containing α-crystals, prepared by two different routes. Direct transformation of the melt at 130 °C, as illustrated with image (B1), caused growth of rather large spherulites, similar as in case of the experiment described with Fig. 5. As demonstrated with the POM image (B2), it is also possible to obtain α-crystals by reorganization of α′-crystals by a solid-solid crystal transformation involving only local-scale rearrangements of the molecular chains in the crystal phase and preserving therefore the microstructure [62,79,106]. For this, sample (A) was annealed in the proximity of the melting temperature of the α′-crystals (150–155 °C [71]) for 20 min. Purpose of preparing PLLA containing α-crystals along different thermal pathways is excluding any effect of the μm-scale morphology on mechanical properties evaluated here. Samples as exemplary shown in the top part of Fig. 7 were then subjected to QCSM nanoindentation experiments, with the obtained hardness and indention modulus shown as a function of the displacement in the lower part of the figure. In addition, a fully amorphous sample was included, prepared by quenching the melt from 220 °C to below T_g, followed by long-term storage at ambient temperature to allow physical aging. The hardness and indentation modulus at each indentation depth are average values based on multiple (6–10) measurements per sample, providing the error bar. The hardness drop at the right side of the curves is depicting the hardness reduction during the creep time of 60 s and the last point of the curve is identical to the results from the conventional analysis of the unloading curve. For all samples of different structure, an indentation-size effect is detected for indentation depths lower than about 0.5–1 μm (see gray shaded displacement range), confirming that data obtained from single-cycle measurements (Fig. 6) are reliable from this point-of-view. Otherwise, also QCSM reveals higher hardness and modulus values for PLLA containing α-crystals, regardless whether grown directly from the melt (red triangles) or formed *via* reorganization of α′-crystals (light-red diamond symbols), compared to PLLA containing α′-crystals (blue circles) or fully amorphous glassy PLLA (black squares).

Table 1 is a summary of hardness and modulus values obtained on hotstage-prepared PLLA samples of different structure, confirming reproducibility and absence of an indentation-size effect when using the standard single-cycle and QCSM test methods. PLLA spherulites containing α-crystals exhibit about 20 % higher hardness and modulus than spherulites containing α′-crystals, or the bulk amorphous glass, subjected to physical aging prior analysis. These results qualitatively confirm studies of phase-sensitive mechanical properties obtained by global/macroscopic mechanical tests reported elsewhere [75,76], and serve as a reference for performing nanoindentation tests on FSC samples described below.

3.2. Nanoindentation tests of FSC samples

Fig. 8 presents temperature-time profiles for preparation of PLLA samples containing different crystal polymorphs using FSC *via* two different crystallization pathways, (c) and (d), as indicated. Crystallization pathway (c) serves for spherulitic growth of α-crystals at 140 °C (see red segment), which, however, is difficult if the crystallization temperature is directly approached by cooling the relaxed melt, related to the low number of nuclei in the tiny FSC samples. For this reason, an additional nucleation step at 60 °C is included in the thermal profile,

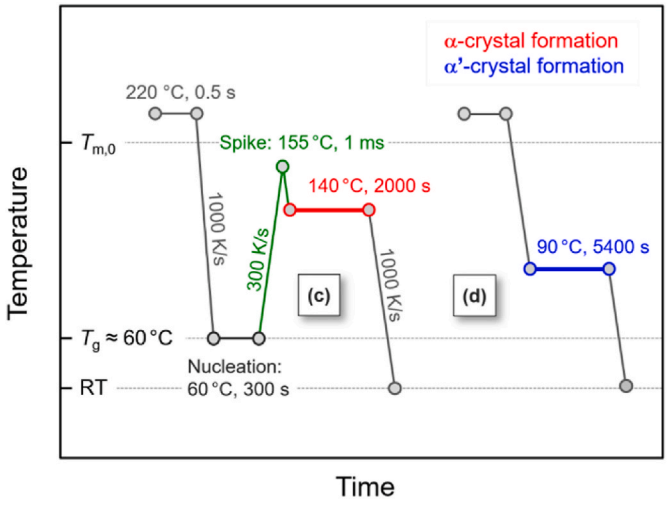

Fig. 8. Temperature-time protocols for preparation of semicrystalline PLLA spherulites on FSC chips, containing both α-crystals and amorphous structure [path (c)], and spherulites containing both α′-crystals and amorphous structure [path (d)].

followed by a further control/fine-tuning of the nuclei number with a short temperature spike on the transfer of nuclei to the growth temperature, to precisely adjust the nuclei number and with that the spherulite size [107–110]. The use of the nucleation path prior to the crystallization process at higher temperatures results in smaller structures due to an increase in the nuclei density and smaller spherulites with a diameter of about 10 μm (not shown). Formation of small spherulites causes a non-smooth and uneven/locally curved sample surface being disadvantageous for nanoindentation measurements. The specific nucleation path used, finally, assured formation of a well-defined number of rather large spherulites, yielding a less curved sample surface. Worth noting that both the nucleation step (60 °C, 300 s) and nuclei-transfer step (green) including the transfer heating rate of 300 K/s and the temperature/time of the spike, were subject of intense prior research for understanding homogeneous crystal nucleation in PLLA, being not chosen arbitrarily. The thermal protocol (d) served for spherulitic growth of α′-crystals, with an additional nucleation step not needed due to the higher —compared to 140 °C— nucleation rate. Importantly, as in case of hotstage-prepared PLLA samples, the local crystallinity of spherulites containing α- and α′-crystals is assumed similar since samples were not subjected to extended secondary crystallization at the temperature of primary crystallization.

Fig. 9 shows POM images of semicrystalline PLLA containing spherulites with α-crystals (left) or α′-crystals (right), together, in both cases, with amorphous structure, prepared on FSC chip sensors *via* the crystallization pathways (c) and (d) (see Fig. 8), respectively. The top right inset provides a full view of the samples, while the main images show the structure at higher resolution. Note that the scale bar holds for both images, (c) and (d). The micrograph of PLLA crystallized at 140 °C (left), containing α-crystals displays large spherulites with a diameter of about 150 μm, adjusted by the specific nucleation path (see left temperature-time protocol in Fig. 8). In case of PLLA crystallized at 90 °C, to allow growth of the α′-phase (right image), spherulites with a diameter of, at best, a few ten μm developed, being typical for PLLA [101].

The samples shown in Fig. 9 served for conduction of nanoindentation measurements using the QCSM mode after loading them onto the sample holder of the nanoindenter device, as described in the experimental section. Multiple indentation experiments in the center area of the samples yielded average values of the hardness and indentation modulus of 0.42 and 5.8 GPa for PLLA-spherulites containing α-crystals and 0.26 and 5.4 GPa for PLLA-spherulites containing

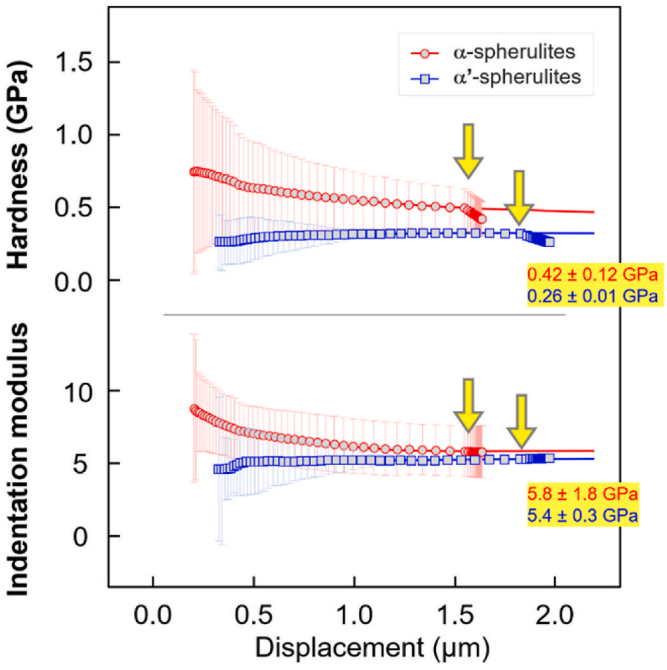

Fig. 10. Hardness (top) and indentation modulus (bottom) of PLLA spherulites containing —beside amorphous structure— α-crystals (red circles) or α′-crystals (blue squares). (For interpretation of the references to colour in this figure legend, the reader is referred to the Web version of this article.)

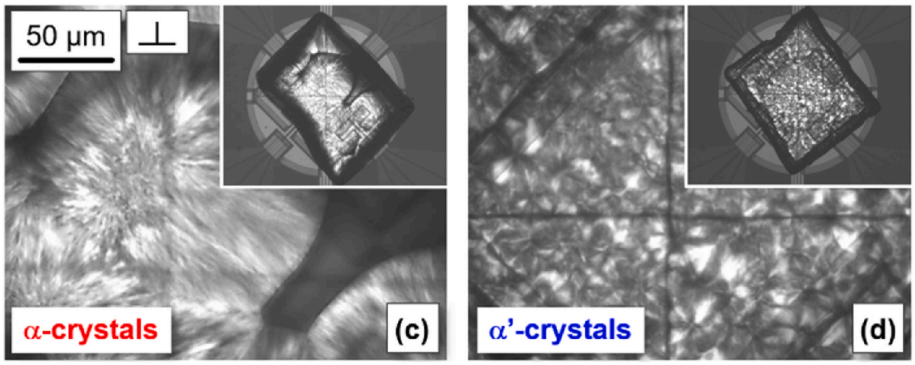

Fig. 9. POM images of PLLA samples prepared in an FSC, crystallized according to the temperature-time protocols/pathways (c) (left) and (d) (right) (for the temperature-time protocols see also Fig. 8). The scale bar holds for both images, and the polarizer directions are oriented parallel to the image borders as indicated in the left image. The insets provide a full view of the samples. The sample thickness is about 20 μm.

α′-crystals, respectively. Fig. 10 shows in the top and bottom parts the hardness and indentation modulus, respectively, for the PLLA spherulites with α-crystals (red circles) and α′-crystals (blue squares) as a function of the displacement, for illustrating the indentation-size effect. For PLLA containing α-crystals, similar as in case of hotstage-prepared samples (see Fig. 7), hardness and modulus decrease with increasing penetration-depth, to approach a plateau value only after about 1.5 μm. In addition, data show large scatter. A reason may be the rather large concave curvature of the sample surface parallel to the radius of the spherulites from the center to their edge, due to the volume shrinkage during crystallization, yielding a thickness-wise uneven though smooth surface. Due to this issue, we often observed asymmetric triangle-shaped impressions complicating the analysis. In contrast, indents in PLLA containing α′-crystals were symmetric, causing less scattering of hardness and modulus values and an indentation-size effect is also not observed. Despite the rather low thickness of the FSC-samples may cause complications, the observed hardness and modulus values are in qualitative agreement with results obtained on both hotstage-prepared samples (see Table 1), and —perhaps even more important— also with the expectations based on independent analyses using different instrumentation (dynamic-mechanical analysis).

4. Summary

The pathway of solidification/crystallization the melt, and related semicrystalline morphologies, affects for many polymers ultimate and application-relevant properties. Therefore, understanding the link between solidification conditions, structure, and properties is a key issue in material development. Many studies focused on analysis of the relation between crystallization conditions and resulting structures at thermal conditions as evident in melt processing, by employing the rather novel fast-scanning-chip calorimetry (FSC) technique and its combination with classical structure-analysis tools. Knowledge of mechanical properties of the typically nanogram-sized samples used in such analyses is absent so far, however, is needed to establish clear-cut structure-property relationships. For this reason, in this work, we used the nanoindentation technique for assessing both hardness and indentation modulus of a typical FSC sample of known crystallization behavior, structure, and mechanical characteristics. We employed PLLA as a test object, known to crystallize in different crystal structures as a function of the crystallization temperature, as well as to fully preserve the amorphous state on fast cooling to below the glass transition temperature. We presented a strategy to prepare samples for the nanoindentation tests, such to transfer the FSC specimen, which solidified on a thin free-standing membrane, onto a solid and stiff steel-substrate, being a prerequisite for the subsequent nanoindentation measurements. With analyses performed on 20 μm thick samples, we were able to reproduce/confirm modulus values of around 5.8 and 5.4 GPa for semicrystalline PLLA spherulites containing either rather perfect (higher density) α- and disorder (lower density) α′-crystals, respectively. With the assumption of a similar local crystal fraction within the spherulites, the observation of a lower modulus of PLLA containing α′-crystals is in agreement with independent, global/macroscopic scale studies.

In conclusion, combining FSC for precise control of crystallization pathways and obtaining of well-defined morphologies in polymers on one side, and nanoindentation for assessing mechanical properties of nanogram-sized samples on the other side, appears promising. However, though first experimentally observed quantitative results agree with expectations, there remain numerous questions, to be subject of further work. Among those, beside instrumental issues, analysis of the effects of crystal orientation, of crystallinity gradients within spherulites, or of different structure and properties in surface-near and -far regions, to name only a few, require further investigations.

CRediT authorship contribution statement

Katalee Jariyavidyanont: Writing – review & editing, Writing – original draft, Investigation, Conceptualization. **Christina Wüstefeld:** Writing – review & editing, Investigation. **Thomas Chudoba:** Writing – review & editing, Investigation. **René Androsch:** Writing – review & editing, Investigation, Conceptualization.

Declaration of competing interest

The authors declare the following financial interests/personal relationships which may be considered as potential competing interests:

Rene Androsch reports financial support was provided by Deutsche Forschungsgemeinschaft (DFG). If there are other authors, they declare that they have no known competing financial interests or personal relationships that could have appeared to influence the work reported in this paper.

Data availability

Data will be made available on request.

Acknowledgement

KJ and RA gratefully acknowledge financial support by the Deutsche Forschungsgemeinschaft (DGF) (grant number AN 212/26).

References

[1] T.A. Osswald, G. Menges, Materials Science of Polymers for Engineers, Hanser, Munich, 2012, https://doi.org/10.3139/9781569905241.
[2] H.W. Starkweather Jr., R.E. Brooks, Effect of spherulites on the mechanical properties of nylon 66, J. Appl. Polym. Sci. 1 (1959) 236–239, https://doi.org/10.1002/app.1959.070010214.
[3] Q. Zia, H.-J. Radusch, R. Androsch, Deformation behavior of isotactic polypropylene crystallized via a mesophase, Polym. Bull. 63 (2009) 755–771, https://doi.org/10.1007/s00289-009-0151-y.
[4] C.D. Rosa, F. Auriemma, R.D. Girolamo, O.R. de Ballesteros, Crystallization of the mesomorphic form and control of the molecular structure for tailoring the mechanical properties of isotactic polypropylene, J. Polym. Sci., Part B: Polym. Phys. 52 (2014) 677–699, https://doi.org/10.1002/polb.23473.
[5] G.B. McKenna, Y. Leterrier, C.R. Schultheisz, The evolution of material properties during physical aging, Polym. Eng. Sci. 35 (1995) 403–410, https://doi.org/10.1002/pen.760350505.
[6] H.M. Naeem Iqbal, C. Sungkapreecha, R. Androsch, Enthalpy relaxation of the glass of poly (L-lactic acid) of different D-isomer content and its effect on mechanical properties, Polym. Bull. 74 (2017) 2565–2573, https://doi.org/10.1007/s00289-016-1854-5.
[7] V. Brucato, S. Piccarolo, V. La Carrubba, An experimental methodology to study polymer crystallization under processing conditions. The influence of high cooling rates, Chem. Eng. Sci. 57 (2002) 4129–4143, https://doi.org/10.1016/S0009-2509(02)00360-3.
[8] D. Cavallo, L. Gardella, G.C. Alfonso, G. Portale, L. Balzano, R. Androsch, Effect of cooling rate on the crystal/mesophase polymorphism of polyamide 6, Colloid, Polym. Sci. 289 (2011) 1073–1079, https://doi.org/10.1007/s00396-011-2428-6.
[9] J.E.K. Schawe, Influence of processing conditions on polymer crystallization measured by fast scanning DSC, J. Therm. Anal. Calorim. 116 (2014) 1165–1173, https://doi.org/10.1007/s10973-013-3563-8.
[10] J.E.K. Schawe, Measurement of the thermal glass transition of polystyrene in a cooling rate range of more than six decades, Thermochim. Acta 603 (2015) 128–134, https://doi.org/10.1016/j.tca.2014.05.025.
[11] S.S. Katti, J.M. Schultz, The microstructure of injection-molded semicrystalline polymers: a review, Polym. Eng. Sci. 22 (1982) 1001–1017, https://doi.org/10.1002/pen.760221602.
[12] R. Pantani, I. Coccorullo, V. Speranza, G. Titomanlio, Modeling of morphology evolution in the injection molding process of thermoplastic polymers, Prog. Polym. Sci. 30 (2005) 1185–1222, https://doi.org/10.1016/j.progpolymsci.2005.09.001.
[13] Y. Spoerer, R. Androsch, D. Jehnichen, I. Kuehnert, Process induced skin-core morphology in injection molded polyamide 66, Polymers 12 (2020) 894, https://doi.org/10.3390/polym12040894.
[14] M.R. Kantz, H.D. Newman, F.H. Stigale, The skin-core morphology and structure–property relationships in injection-molded polypropylene, J. Appl. Polym. Sci. 16 (1972) 1249–1260, https://doi.org/10.1002/app.1972.070160516.

[15] E. Hnatkova, Z. Dvorak, Effect of the skin-core morphology on the mechanical properties of injection-moulded parts, Mater. Technol. 50 (2016) 195–198, https://doi.org/10.17222/mit.2014.151.
[16] R. Čermák, M. Obadal, P. Ponížil, M. Polášková, K. Stoklasa, A. Lengálová, Injection-moulded α- and β-polypropylenes: I. Structure vs. processing parameters, Eur. Polym. J. 41 (2005) 1838–1845, https://doi.org/10.1016/j.eurpolymj.2005.02.020.
[17] K. Maeda, K. Yamada, K. Yamada, M. Kotaki, H. Nishimura, The relationship between bulk property and property distribution in thin-wall injection molded PP at different molecular weight and molecular weight distribution, Adv. Mater. Phys. Chem. 6 (2016) 1–8, https://doi.org/10.4236/ampc.2016.61001.
[18] N. Mahmood, I. Kolesov, R. Gluege, H. Altenbach, R. Androsch, M. Beiner, Influence of structure gradients in injection moldings of isotactic polypropylene on their mechanical properties, Polymer 200 (2020) 122556, https://doi.org/10.1016/j.polymer.2020.122556.
[19] S. Liparoti, R. Salomone, V. Speranza, R. Pantani, Morphology distribution in injection molded parts, Polymers 16 (2024) 337, https://doi.org/10.3390/polym16030337.
[20] Y. Kobayashi, H. Kanno, Y. Hanamoto, M. Ando, T. Kanai, Relating microhardness to injection molding induced morphology: a study of microbeam synchrotron WAXD, J. Appl. Polym. Sci. 116 (2010) 1823–1831, https://doi.org/10.1002/app.31719.
[21] R. Lesan-Khosh, R. Bagheri, S. Asgari, Nanoindentation of isotactic polypropylene: correlations between hardness, yield stress, and modulus on the local and global scales, J. Appl. Polym. Sci. 121 (2011) 930–938, https://doi.org/10.1002/app.33635.
[22] S. Liparoti, A. Sorrentino, V. Speranza, G. Titomanlio, Multiscale mechanical characterization of iPP injection molded samples, Eur. Polym. J. 90 (2017) 79–91, https://doi.org/10.1016/j.eurpolymj.2017.03.010.
[23] D. Mileva, Q. Zia, R. Androsch, Tensile properties of random copolymers of propylene with ethylene and 1-butene: effect of crystallinity and crystal habit, Polym. Bull. 65 (2010) 623–634, https://doi.org/10.1007/s00289-010-0274-1.
[24] I. Kolesov, D. Mileva, R. Androsch, Mechanical behavior and optical transparency of polyamide 6 of different morphology formed by variation of the pathway of crystallization, Polym. Bull. 71 (2014) 581–593, https://doi.org/10.1007/s00289-013-1079-9.
[25] M. Cocca, M.L. Di Lorenzo, M. Malinconico, V. Frezza, Influence of crystal polymorphism on mechanical and barrier properties of poly (L-lactic acid), Eur. Polym. J. 47 (2011) 1073–1080, https://doi.org/10.1016/j.eurpolymj.2011.02.009.
[26] C. De Rosa, F. Auriemma, R. Di Girolamo, O. Ruiz de Ballesteros, M. Pepe, O. Tarallo, A. Malafronte, Morphology and mechanical properties of the mesomorphic form of isotactic polypropylene in stereodefective polypropylene, Macromolecules 46 (2013) 5202–5214, https://doi.org/10.1021/ma400570k.
[27] C. Schick, V. Mathot, Fast Scanning Calorimetry, Springer, Cham, 2016, https://doi.org/10.1007/978-3-319-31329-0.
[28] A.A. Minakov, C. Schick, Ultrafast thermal processing and nanocalorimetry at heating and cooling rates up to 1 MK/s, Rev. Sci. Instrum. 78 (2007) 073902, https://doi.org/10.1063/1.2751411.
[29] A. Minakov, J. Morikawa, E. Zhuravlev, M. Ryu, A.W. Van Herwaarden, C. Schick, High-speed dynamics of temperature distribution in ultrafast (up to 10^8 K/s) chip-nanocalorimeters, measured by infrared thermography of high resolution, J. Appl. Phys. 125 (2019) 054501, https://doi.org/10.1063/1.5066384.
[30] A. Sorrentino, F. De Santis, G. Titomanlio, Polymer crystallization under high cooling rate and pressure: a step towards polymer processing conditions, in: G. Reiter, G.R. Strobl (Eds.), Progress in Understanding of Polymer Crystallization, Lecture Notes in Physics, vol. 714, Springer, Berlin, Heidelberg, 2007, pp. 329–344, https://doi.org/10.1007/3-540-47307-6_16.
[31] E. Parodi, G.W. Peters, L.E. Govaert, Structure-properties relations for polyamide 6, Part 2: influence of processing conditions during injection moulding on deformation and failure kinetics, Polymers 10 (2018) 779, https://doi.org/10.3390/polym10070779.
[32] D.P. Russell, P.W. Beaumont, Structure and properties of injection-moulded nylon-6, Part 1: Structure and morphology of nylon-6, J. Mater. Sci. 15 (1980) 197–207, https://doi.org/10.1007/BF00552445.
[33] K. Jariyavidyanont, J.L. Williams, A.M. Rhoades, I. Kühnert, W. Focke, R. Androsch, Crystallization of polyamide 11 during injection molding, Polym. Eng. Sci. 58 (2018) 1053–1061, https://doi.org/10.1002/pen.24665.
[34] M. Du, K. Jariyavidyanont, R. Boldt, M. Tariq, M. Fischer, Y. Spoerer, I. Kuehnert, R. Androsch, Crystal-nuclei formation during injection-molding of poly (L-lactic acid), Polymer 250 (2022) 124897, https://doi.org/10.1016/j.polymer.2022.124897.
[35] G.W.H. Höhne, W. Hemminger, H.-J. Flammersheim, Differential Scanning Calorimetry, Springer, Berlin, Heidelberg, 1996, https://doi.org/10.1007/978-3-662-03302-9_1.
[36] R. Androsch, M.L. Di Lorenzo, C. Schick, Optical microscopy to study crystal nucleation in polymers using a fast scanning chip calorimeter for precise control of the nucleation pathway, Macromol. Chem. Phys. 219 (2018) 1700479, https://doi.org/10.1002/macp.201700479.
[37] A.P. Melnikov, D.A. Ivanov, Detecting reorganization in semicrystalline polymers during heating: insights from fast scanning chip calorimetry coupled with real-time optical microscopy, Thermochim. Acta 733 (2024) 179697, https://doi.org/10.1016/j.tca.2024.179697.
[38] K. Jariyavidyanont, R. Zhang, Q. Yu, A. Janke, T. Thurn-Albrecht, C. Schick, R. Androsch, Formation of imperfect crystals in poly(ε-caprolactone) at high melt-supercooling, Mater. Lett. 324 (2022) 132704, https://doi.org/10.1016/j.matlet.2022.132704.
[39] R. Androsch, K. Jariyavidyanont, A. Janke, C. Schick, Poly (butylene succinate): low-temperature nucleation and crystallization, complex morphology and absence of lamellar thickening, Polymer 285 (2023) 126311, https://doi.org/10.1016/j.polymer.2023.126311.
[40] M. Molina-Ruiz, A.F. Lopeandía, F. Pi, D. Givord, O. Bourgeois, J. Rodríguez-Viejo, Evidence of finite-size effect on the Néel temperature in ultrathin layers of CoO nanograins, Phys. Rev. B 83 (2011) 140407, https://doi.org/10.1103/PhysRevB.83.140407.
[41] M.D. Grapes, T. LaGrange, L.H. Friedman, B.W. Reed, G.H. Campbell, T.P. Weihs, D.A. LaVan, Combining nanocalorimetry and dynamic transmission electron microscopy for in situ characterization of materials processes under rapid heating and cooling, Rev. Sci. Instrum. 85 (2014) 084902, https://doi.org/10.1063/1.4892537.
[42] K. Xiao, J.M. Gregoire, P.J. McCluskey, D. Dale, J.J. Vlassak, Scanning AC nanocalorimetry combined with in-situ x-ray diffraction, J. Appl. Phys. 113 (2013) 243501, https://doi.org/10.1063/1.4811686.
[43] D. Baeten, V.B.F. Mathot, T.F.J. Pijpers, O. Verkinderen, G. Portale, P. Van Puyvelde, B. Goderis, Simultaneous synchrotron WAXD and fast scanning (chip) calorimetry: on the (isothermal) crystallization of HDPE and PA11 at high supercoolings and cooling rates up to 200 °C s^{-1}, Macromol. Rapid Commun. 36 (2015) 1184–1191, https://doi.org/10.1002/marc.201500081.
[44] A. Toda, K. Taguchi, K. Nozaki, Gibbs–Thomson, thermal Gibbs–Thomson, and Hoffman–Weeks plots of polyethylene crystals examined by fast-scan calorimetry and small-angle X-ray scattering, Cryst. Growth Des. 19 (2019) 2493–2502, https://doi.org/10.1021/acs.cgd.9b00209.
[45] A.M. Anton, E. Zhuravlev, W. Kossack, R. Andrianov, C. Schick, F. Kremer, Fingerprints of homogeneous nucleation and crystal growth in polyamide 66 as studied by combined infrared spectroscopy and fast scanning chip calorimetry, Colloid Polym. Sci. 298 (2020) 697–706, https://doi.org/10.1007/s00396-020-04666-9.
[46] W.K. Kipnusu, E. Zhuravlev, C. Schick, F. Kremer, The initial molecular interactions in the course of enthalpy relaxation and nucleation in polyethylene terephthalate (PET) as monitored by combined nanocalorimetry and FTIR spectroscopy, Macromol. Chem. Phys. 224 (2023) 2200443, https://doi.org/10.1002/macp.202200443.
[47] Y.I. Golovin, Nanoindentation and mechanical properties of materials at submicro- and nanoscale levels: recent results and achievements, Phys. Solid State 63 (2021) 1–41, https://doi.org/10.1134/S1063783421010108.
[48] H. Wang, L. Zhu, B. Xu, Principle and methods of nanoindentation test, in: H. Wang, L. Zhu, B. Xu (Eds.), Residual Stresses and Nanoindentation Testing of Films and Coatings, Springer, Singapore, 2018, pp. 21–36, https://doi.org/10.1007/978-981-10-7841-5_2.
[49] S.E. Arevalo, D.M. Ebenstein, L.A. Pruitt, A methodological framework for nanomechanical characterization of soft biomaterials and polymers, J. Mech. Behav. Biomed. Mater. 134 (2022) 105384, https://doi.org/10.1016/j.jmbbm.2022.105384.
[50] E. Balla, V. Daniilidis, G. Karlioti, T. Kalamas, M. Stefanidou, N.D. Bikiaris, A. Vlachopoulos, I. Koumentakou, D.N. Bikiaris, Poly(lactic Acid): a versatile biobased polymer for the future with multifunctional properties—from monomer synthesis, polymerization techniques and molecular weight increase to PLA applications, Polymers 13 (2021) 1822, https://doi.org/10.3390/polym13111822.
[51] R. Auras, L.-T. Lim, S.E.M. Selke, H. Tsuji (Eds.), Poly (Lactic Acid): Synthesis, Structures, Properties, Processing, and Applications, Wiley, Hoboken, 2010, https://doi.org/10.1002/9780470649848.
[52] M.L. Di Lorenzo, R. Androsch (Eds.), Synthesis, Structure and Properties of Poly (lactic acid), Springer, Cham, 2018, https://doi.org/10.1007/978-3-319-64230-7.
[53] M. Pyda, R.C. Bopp, B. Wunderlich, Heat capacity of poly(lactic acid), J. Chem. Thermodyn. 36 (2004) 731–742, https://doi.org/10.1016/j.jct.2004.05.003.
[54] S. Saeidlou, M.A. Huneault, H. Li, C.B. Park, Poly(lactic acid) crystallization, Prog. Polym. Sci. 37 (2012) 1657–1677, https://doi.org/10.1016/j.progpolymsci.2012.07.005.
[55] R. Zhang, F. Du, K. Jariyavidyanont, E. Zhuravlev, C. Schick, R. Androsch, Glass transition temperature of poly(D,L-lactic acid) of different molar mass, Thermochim. Acta 718 (2022) 179387, https://doi.org/10.1016/j.tca.2022.179387.
[56] A. Toda, R. Androsch, C. Schick, Insights into polymer crystallization and melting from fast scanning chip calorimetry, Polymer 91 (2016) 239–263, https://doi.org/10.1016/j.polymer.2016.03.038.
[57] H. Li, M.A. Huneault, Effect of nucleation and plasticization on the crystallization of poly(lactic acid), Polymer 48 (2007) 6855–6866, https://doi.org/10.1016/j.polymer.2007.09.020.
[58] R. Androsch, C. Schick, M.L. Di Lorenzo, Kinetics of nucleation and growth of crystals of poly(L-lactic acid), Adv. Polym. Sci. 279 (2018) 235–272, https://doi.org/10.1007/12_2016_13.
[59] P. Pan, Y. Inoue, Polymorphism and isomorphism in biodegradable polyesters, Prog. Polym. Sci. 34 (2009) 605–640, https://doi.org/10.1016/j.progpolymsci.2009.01.003.
[60] B. Lotz, Crystal polymorphism and morphology of polylactides, Adv. Polym. Sci. 279 (2018) 273–302, https://doi.org/10.1007/12_2016_15.
[61] J. Zhang, Y. Duan, H. Sato, H. Tsuji, I. Noda, S. Yan, Y. Ozaki, Crystal modifications and thermal behavior of poly(L-lactic acid) revealed by infrared

spectroscopy, Macromolecules 38 (2005) 8012–8021, https://doi.org/10.1021/ma051232r.
[62] P. Pan, W. Kai, B. Zhu, T. Dong, Y. Inoue, Polymorphous crystallization and multiple melting behavior of poly(L-lactide): molecular weight dependence, Macromolecules 40 (2007) 6898–6905, https://doi.org/10.1021/ma071258d.
[63] J. Zhang, K. Tashiro, H. Tsuji, A.J. Domb, Disorder-to-order phase transition and multiple melting behavior of poly(L-lactide) investigated by simultaneous measurements of WAXD and DSC, Macromolecules 41 (2008) 1352–1357, https://doi.org/10.1021/ma0706071.
[64] P. De Santis, A.J. Kovacs, Molecular conformation of poly(S-lactic acid), Biopolymers 6 (1968) 299–306, https://doi.org/10.1002/bip.1968.360060305.
[65] K. Wasanasuk, K. Tashiro, M. Hanesaka, T. Ohhara, K. Kurihara, R. Kuroki, T. Tamada, T. Ozeki, T. Kanamoto, Crystal structure analysis of poly(L-lactic acid) α form on the basis of the 2-dimensional wide-angle synchrotron X-ray and neutron diffraction measurements, Macromolecules 44 (2011) 6441–6452, https://doi.org/10.1021/ma2006624.
[66] K. Wasanasuk, K. Tashiro, Crystal structure and disorder in poly(L-lactic acid) δ form (α′ form) and the phase transition mechanism to the ordered α form, Polymer 52 (2011) 6097–6109, https://doi.org/10.1016/j.polymer.2011.10.046.
[67] T. Kawai, N. Rahman, G. Matsuba, K. Nishida, T. Kanaya, M. Nakano, H. Okamoto, J. Kawada, A. Usuki, N. Honma, K. Nakajima, M. Matsuda, Crystallization and melting behavior of poly (L-lactic acid), Macromolecules 40 (2007) 9463–9469, https://doi.org/10.1021/ma070082c.
[68] J.P. Kalish, K. Aou, X. Yang, S.L. Hsu, Spectroscopic and thermal analyses of α′ and α crystalline forms of poly(L-lactic acid), Polymer 52 (2011) 814–821, https://doi.org/10.1016/j.polymer.2010.12.042.
[69] J. Zhang, K. Tashiro, A.J. Domb, H. Tsuji, Confirmation of disorder α form of poly (L-lactic acid) by the X-ray fiber pattern and polarized IR/Raman spectra measured for uniaxially-oriented samples, Macromol. Symp. 242 (2006) 274–278, https://doi.org/10.1002/masy.200651038.
[70] M.L. Di Lorenzo, M. Cocca, M. Malinconico, Crystal polymorphism of poly(L-lactic acid) and its influence on thermal properties, Thermochim. Acta 522 (2011) 110–117, https://doi.org/10.1016/j.tca.2010.12.027.
[71] R. Androsch, C. Schick, M.L. Di Lorenzo, Melting of conformationally disordered crystals (α′-phase) of poly(L-lactic acid), Macromol. Chem. Phys. 215 (2014) 1134–1139, https://doi.org/10.1002/macp.201400126.
[72] K. Jariyavidyanont, C. Schick, R. Androsch, The bulk enthalpy of melting of α'-crystals of poly (L-lactic acid) determined by fast scanning chip calorimetry, Thermochim. Acta 717 (2022) 179349, https://doi.org/10.1016/j.tca.2022.179349.
[73] M. Cocca, R. Androsch, M.C. Righetti, M. Malinconico, M.L. Di Lorenzo, Conformationally disordered crystals and their influence on material properties: the cases of isotactic polypropylene, isotactic poly(1-butene), and poly(L-lactic acid), J. Mol. Struct. 1078 (2014) 114–132, https://doi.org/10.1016/j.molstruc.2014.02.038.
[74] M. Cocca, M.L. Di Lorenzo, M. Malinconico, V. Frezza, Influence of crystal polymorphism on mechanical and barrier properties of poly(L-lactic acid), Eur. Polym. J. 47 (2011) 1073–1080, https://doi.org/10.1016/j.eurpolymj.2011.02.009.
[75] L. Aliotta, M. Gazzano, A. Lazzeri, M.C. Righetti, Constrained amorphous interphase in poly(L-lactic acid): estimation of the tensile elastic modulus, ACS Omega 5 (2020) 20890–20902, https://doi.org/10.1021/acsomega.0c02330.
[76] K. Jariyavidyanont, Q. Yu, A. Petzold, T. Thurn-Albrecht, R. Glüge, H. Altenbach, R. Androsch, Young's modulus of the different crystalline phases of poly (L-lactic acid), J. Mech. Behav. Biomed. Mater. 137 (2023) 105546, https://doi.org/10.1016/j.jmbbm.2022.105546.
[77] K. Wasanasuk, K. Tashiro, Theoretical and experimental evaluation of crystallite moduli of various crystalline forms of poly(L-lactic acid), Macromolecules 45 (2012) 7019–7026, https://doi.org/10.1021/ma3010982.
[78] T. Lin, X.Y. Liu, C. He, Ab initio elasticity of poly(lactic acid) crystals, J. Phys. Chem. B 114 (2010) 3133–3139, https://doi.org/10.1021/jp911198p.
[79] K. Jariyavidyanont, A. Janke, Q. Yu, T. Thurn-Albrecht, R. Androsch, Lamellar morphology of disorder α′-crystals of poly(L-lactic acid), Cryst. Growth Des. 24 (2024) 1825–1834, https://doi.org/10.1021/acs.cgd.3c01498.
[80] P. Pan, B. Zhu, Y. Inoue, Enthalpy relaxation and embrittlement of poly(L-lactide) during physical aging, Macromolecules 40 (2007) 9664–9671, https://doi.org/10.1021/ma071737c.
[81] L. Cui, B. Imre, D. Tátraaljai, B. Pukánszky, Physical ageing of poly(lactic acid): factors and consequences for practice, Polymer 186 (2020) 122014, https://doi.org/10.1016/j.polymer.2019.122014.
[82] Y. Wang, J.F. Mano, Effect of structural relaxation at physiological temperature on the mechanical property of poly(L-lactic acid) studied by microhardness measurements, J. Appl. Polym. Sci. 100 (2006) 2628–2633, https://doi.org/10.1002/app.22643.
[83] Total-Corbion, Product data sheet. https://www.totalenergies-corbion.com/media/dtnoqxkb/pds-luminy-l175-20220722.pdf. (Accessed 19 February 2024).
[84] Corbion, Personal Information, 2018, 10/08.
[85] Flash DSC 2+ Operating Instructions, Mettler-Toledo, Greifensee, Switzerland.
[86] V. Mathot, M. Pyda, T. Pijpers, G.V. Poel, E. van de Kerkhof, S. van Herwaarden, F. van Herwaarden, A. Leenaers, The Flash DSC 1, a power compensation twin-type, chip-based fast scanning calorimeter (FSC): first findings on polymers, Thermochim. Acta 522 (2011) 36–45, https://doi.org/10.1016/j.tca.2011.02.031.
[87] S. van Herwaarden, E. Iervolino, F. van Herwaarden, T. Wijffels, A. Leenaers, V. Mathot, Design, performance and analysis of thermal lag of the UFS1 twin-calorimeter chip for fast scanning calorimetry using the Mettler-Toledo Flash DSC 1, Thermochim. Acta 522 (2011) 46–52, https://doi.org/10.1016/j.tca.2011.05.025.
[88] K. Jariyavidyanont, A. Abdelaziz, R. Androsch, C. Schick, Experimental analysis of lateral thermal inhomogeneity of a specific chip-calorimeter sensor, Thermochim. Acta 674 (2019) 95–99, https://doi.org/10.1016/j.tca.2019.02.016.
[89] G.V. Poel, D. Istrate, A. Magon, V. Mathot, Performance and calibration of the Flash DSC 1, a new, MEMS-based fast scanning calorimeter, J. Therm. Anal. Calorim. 110 (2012) 1533–1546, https://doi.org/10.1007/s10973-012-2722-7.
[90] I. Kolesov, D. Mileva, R. Androsch, C. Schick, Structure formation of polyamide 6 from the glassy state by fast scanning chip calorimetry, Polymer 52 (2011) 5156–5165, https://doi.org/10.1016/j.polymer.2011.09.007.
[91] A.M. Rhoades, N. Wonderling, A. Gohn, J. Williams, D. Mileva, M. Gahleitner, R. Androsch, Effect of cooling rate on crystal polymorphism in beta-nucleated isotactic polypropylene as revealed by a combined WAXS/FSC analysis, Polymer 90 (2016) 67–75, https://doi.org/10.1016/j.polymer.2016.02.047.
[92] X. Li, B. Bhushan, A review of nanoindentation continuous stiffness measurement technique and its applications, Mater. Charact. 48 (2002) 11–36, https://doi.org/10.1016/S1044-5803(02)00192-4.
[93] M. Egart, B. Janković, S. Srčič, Application of instrumented nanoindentation in preformulation studies of pharmaceutical active ingredients and excipients, Acta Pharm. 66 (2016) 303–330, https://doi.org/10.1515/acph-2016-0032.
[94] L. Lorenz, T. Chudoba, S. Makowski, M. Zawischa, F. Schaller, V. Weihnacht, Indentation modulus extrapolation and thickness estimation of ta-C coatings from nanoindentation, J. Mater. Sci. 56 (2021) 18740–18748, https://doi.org/10.1007/s10853-021-06448-2.
[95] T. Chudoba, D. Schwenk, P. Reinstädt, M. Griepentrog, High-precision calibration of indenter area function and instrument compliance, JOM 74 (2022) 2179–2194, https://doi.org/10.1007/s11837-022-05291-3.
[96] W.C. Oliver, G.M. Pharr, An improved technique for determining hardness and elastic modulus using load and displacement sensing indentation experiments, J. Mater. Res. 7 (1992) 1564–1583, https://doi.org/10.1557/JMR.1992.1564.
[97] T. Chudoba, Measurement of hardness and Young's modulus by nanoindentation, in: A. Cavaleiro, J.T.M. De Hosson (Eds.), Nanostructured Coatings, Springer, New York, NY, 2006, pp. 216–260, https://doi.org/10.1007/978-0-387-48756-4_6.
[98] ISO 14577, Metallic Materials - Instrumented Indentation Test for Hardness and Materials Parameters, ISO Central Secretariat, Geneva, Switzerland, 2015.
[99] R. Androsch, H.M.N. Iqbal, C. Schick, Non-isothermal crystal nucleation of poly (L-lactic acid), Polymer 81 (2015) 151–158, https://doi.org/10.1016/j.polymer.2015.11.006.
[100] M. Salmerón Sánchez, V.B.F. Mathot, G. Vanden Poel, J.L. Gómez Ribelles, Effect of the cooling rate on the nucleation kinetics of poly(L-lactic acid) and its influence on morphology, Macromolecules 40 (2007) 7989–7997, https://doi.org/10.1021/ma0712706.
[101] M. Yasuniwa, S. Tsubakihara, K. Iura, Y. Ono, Y. Dan, K. Takahashi, Crystallization behavior of poly(L-lactic acid), Polymer 47 (2006) 7554–7563, https://doi.org/10.1016/j.polymer.2006.08.054.
[102] J. Molnár, A. Hertner-Horváth, A. Menyhárd, Prediction of tensile modulus from calorimetric melting curves of polylactic acid with pronounced cold crystallization ability, Polym. Test. 95 (2021) 107112, https://doi.org/10.1016/j.polymertesting.2021.107112.
[103] R. Rodríguez, I. Gutierrez, Correlation between nanoindentation and tensile properties: influence of the indentation size effect, Mater. Sci. Eng: A 361 (2003) 377–384, https://doi.org/10.1016/S0921-5093(03)00563-X.
[104] G.M. Pharr, E.G. Herbert, Y. Gao, The indentation size effect: a critical examination of experimental observations and mechanistic interpretations, Annu. Rev. Mater. Res. 40 (2010) 271–292, https://doi.org/10.1146/annurev-matsci-070909-104456.
[105] Y.V. Milman, A.A. Golubenko, S.N. Dub, Indentation size effect in nanohardness, Acta Mater. 59 (2011) 7480–7487, https://doi.org/10.1016/j.actamat.2011.08.027.
[106] P. Pan, B. Zhu, W. Kai, T. Dong, Y. Inoue, Polymorphic transition in disordered poly(L-lactide) crystals induced by annealing at elevated temperatures, Macromolecules 41 (2008) 4296–4304, https://doi.org/10.1021/ma800343g.
[107] R. Androsch, M.L. Di Lorenzo, Crystal nucleation in glassy poly(L-lactic acid), Macromolecules 46 (2013) 6048–6056, https://doi.org/10.1021/ma401036j.
[108] R.A. Andrianov, R. Androsch, R. Zhang, T.A. Mukhametzyanov, A.S. Abyzov, J.W.P. Schmelzer, C. Schick, Growth and dissolution of crystal nuclei in poly(l-lactic acid) (PLLA) in Tammann's development method, Polymer 196 (2020) 122453, https://doi.org/10.1016/j.polymer.2020.122453.
[109] R.A. Andrianov, J.W.P. Schmelzer, R. Androsch, T.A. Mukhametzyanov, C. Schick, Radial growth rate of near-critical crystal nuclei in poly(L-lactic acid) (PLLA) in Tammann's two-stage development method, J. Chem. Phys. 158 (2023) 054504, https://doi.org/10.1063/5.0134462.
[110] S. Quattrosoldi, N. Lotti, M. Soccio, C. Schick, R. Androsch, Stability of crystal nuclei of poly (butylene isophthalate) formed near the glass transition temperature, Polymers 12 (2020) 1099, https://doi.org/10.3390/polym12051099.